Supplementary

An operational global L-band soil moisture and vegetation optical depth dataset from optimized 40° SMOS brightness temperatures

Zanpin Xing[1,3,4], Xiaojun Li[*2,5], Frédéric Frappart[2], Gabrielle De Lannoy[6], Thomas Jagdhuber[7,8], Jian Peng[9,10], Lei Fan[11], Hongliang Ma[12], Karthikeyan Lanka[13,14], Xiangzhuo Liu[2], Mengjia Wang[2,15], Lin Zhao[16], Yongqin Liu[1,3,4], Jean-Pierre Wigneron[2]

[1]Center for Pan-third Pole Environment, Lanzhou University, Lanzhou, China

[2]INRAE, Bordeaux Sciences Agro, UMR 1391 ISPA, Villenave-d'Ornon, France

[3]Key Laboratory of Pan-third Pole Biogeochemical Cycling, Lanzhou, China

[4]Chayu integrated observation and research station of the Xizang Autonomous Region，Xizang, China

[5]Faculty of Geosciences and Engineering, Southwest Jiaotong University, Chengdu 611756, China

[6]Department of Earth and Environmental Sciences, KU Leuven, Heverlee B-3001, Belgium

[7]German Aerospace Center (DLR) Microwaves and Radar Institute Weßling, Germany

[8]Institute of Geography University of Augsburg (UniA) Augsburg, Germany

[9]Department of Remote Sensing, Helmholtz Centre for Environmental Research - UFZ, Leipzig, Germany

[10]Remote Sensing Centre for Earth System Research-RSC4Earth, Leipzig University, Leipzig, Germany

[11]Chongqing Jinfo Mountain Karst Ecosystem National Observation and Research Station, School of Geographical Sciences, Southwest University, Chongqing, China

[12]INRAE, UMR 1114 EMMAH, UMT CAPTE, Provence-Alpes-Cote d'Azur, F-84000 Avignon, France

[13]Centre of Studies in Resources Engineering, Indian Institute of Technology Bombay, Mumbai, India

[14]Centre for Climate Studies, Indian Institute of Technology Bombay, Mumbai, India

[15]School of Geo-Science and Technology, Zhengzhou University, Zhengzhou 450001, China

[16]School of Geographical Sciences, Nanjing University of Information Science & Technology, Nanjing 210044, China

Corresponding author: Xiaojun Li (xiaojunli_vod@163.com)

Table S1 Summary of the *in-situ* networks from ISMN used in the study. The number of stations/pixels included in each IGBP land cover is also listed.

Network name	**Country**	**No. footprints**	**IGBP land cover types (No.)**
AMMA-CATCH	Benin, Niger	2	S (1) and G (1)
ARM	USA	15	G (6) and C (9)
FMI	Finland	2	WS (2)
FR-Aqui	France	1	ENF (1)
HOAL	Austria	1	MF (1)
HOBE	Denmark	3	C (3)
NAQU	China	1	G (1)
OZNET	Australia	11	S (2) and C (9)
PBO-H2O	USA	1	G (1)
REMEDHUS	Spain	4	S (3) and C (1)
RISMA	Canada	7	C (7)
RSMN	Romania	14	C (12)
SCAN	USA	129	Diverse land cover types: ENF (3), DBF (10), MF (3), OS (31), WS (3), G (46), C (31) and Barren (2)
SMN-SDR	China	1	G (1)
SMOSMANIA	France	17	Diverse land cover types: ENF (2), MF (5), C (9) and CNVM (1)
SNOTEL	USA	172	Diverse land cover types: ENF (63), OS (19), WS (6), G (79) and C (5)
SOILSCAPE	USA	4	Diverse land cover types: OS (2), WS (1) and S (1)
TAHMO	Côte d'Ivoire, Nigeria, Ghana, Uganda, Rwanda, Kenya	3	EBF(2) and WS (1)
TERENO	Germany	1	MF (1)
TWENTE	Netherlands	4	C (4)
TxSON	USA	6	G (6)
USCRN	USCRN	64	Diverse land cover types: ENF (4), DBF (6), MF (1), CS(1), OS (8), WS (2), G (38), C (13) and Barren (1)
iRON	Canada	1	ENF (1)

Table S2 Statistics of validation results of $IB\_HR_{mono}^{SMOSIB}$, IB_{mono}^{SMOSIB}, $IB_{mono}^{RawSMOS}$, IC_{multi}^{SMOS} and IB_{mono}^{SMAP} against ISMN *in-situ* SM data for 2016–2022. Best performance in terms of R, *ub*RMSD and Bias of the five SM retrievals in each network is typed in bold.

Metrics	R					*ub*RMSD (m^3/m^3)					Bias (m^3/m^3)				
Networks	$IB\_HR_{mono}^{SMOSIB}$	IB_{mono}^{SMOSIB}	$IB_{mono}^{RawSMOS}$	IC_{multi}^{SMOS}	IB_{mono}^{SMAP}	$IB\_HR_{mono}^{SMOSIB}$	IB_{mono}^{SMOSIB}	$IB_{mono}^{RawSMOS}$	IC_{multi}^{SMOS}	IB_{mono}^{SMAP}	$IB\_HR_{mono}^{SMOSIB}$	IB_{mono}^{SMOSIB}	$IB_{mono}^{RawSMOS}$	IC_{multi}^{SMOS}	IB_{mono}^{SMAP}
AMMA-CATCH	0.89	**0.90**	0.87	0.88	0.90	**0.024**	0.025	0.030	0.030	0.026	**0.000**	0.012	0.012	0.014	0.013
ARM	0.85	**0.85**	0.84	0.84	0.85	**0.043**	0.044	0.046	0.046	0.044	-0.069	-0.069	-0.068	**-0.064**	-0.069
FMI	0.48	0.46	0.36	0.49	**0.51**	0.043	0.041	0.053	0.058	**0.038**	**0.031**	0.060	0.128	0.103	0.082
FR-Aqui	0.82	0.81	0.78	0.77	**0.86**	0.035	0.035	0.037	0.043	**0.030**	-0.066	-0.047	-0.063	-0.032	**-0.024**
HOAL	0.67	0.64	0.46	0.61	**0.74**	0.044	0.046	0.054	0.050	**0.040**	-0.182	-0.171	-0.188	-0.156	**-0.116**
HOBE	0.68	0.68	0.63	0.64	**0.73**	**0.038**	0.039	0.051	0.047	0.041	-0.071	-0.070	-0.065	**-0.063**	-0.066
NAQU	0.80	0.80	0.79	0.76	**0.86**	0.054	0.057	0.054	0.064	**0.053**	0.057	0.059	0.054	0.066	**0.048**
OZNET	0.76	0.76	0.75	0.73	**0.76**	**0.059**	0.060	0.065	0.067	0.060	-0.018	-0.008	-0.007	**-0.004**	-0.009
PBO-H2O	0.85	0.85	0.81	0.85	**0.87**	0.067	0.067	0.068	**0.062**	0.063	-0.081	-0.082	-0.081	**-0.078**	-0.080
REMEDHUS	0.79	**0.80**	0.79	0.78	0.79	**0.046**	0.047	0.049	0.051	0.047	-0.033	-0.024	-0.024	-0.022	**-0.020**
RISMA	0.63	**0.63**	0.58	0.62	0.61	**0.062**	0.064	0.070	0.074	0.068	-0.096	-0.083	-0.083	**-0.077**	-0.084
RSMN	0.62	0.62	0.53	0.61	**0.62**	0.060	0.061	0.068	0.072	**0.058**	-0.011	**-0.001**	-0.011	0.005	0.002
SCAN	0.67	**0.67**	0.64	0.66	0.66	0.052	**0.052**	0.056	0.057	0.053	-0.049	-0.039	-0.037	**-0.034**	-0.040
SMN-SDR	0.57	0.57	**0.58**	0.58	0.48	0.034	**0.035**	0.039	0.040	0.039	-0.115	-0.114	-0.110	-0.110	**-0.097**
SMOSMANIA	**0.73**	0.73	0.67	0.72	0.75	0.063	0.061	0.062	**0.058**	0.057	-0.104	-0.090	-0.112	-0.074	**-0.074**
SNOTEL	**0.62**	0.62	0.56	0.58	0.60	**0.075**	0.075	0.077	0.078	0.075	-0.088	-0.084	-0.083	**-0.077**	-0.085
SOILSCAPE	0.86	0.86	0.84	0.86	**0.87**	**0.039**	0.041	0.054	0.042	0.041	-0.032	-0.019	**-0.010**	-0.016	-0.014
TAHMO	0.67	0.67	0.63	0.63	**0.71**	**0.039**	0.041	0.047	0.046	0.040	-0.039	-0.027	-0.028	**-0.025**	-0.027
TERENO	0.78	**0.78**	0.67	0.75	0.78	0.057	0.055	0.063	0.056	**0.055**	-0.191	-0.169	-0.167	**-0.162**	-0.169
TWENTE	0.75	0.75	0.69	0.73	**0.77**	0.063	0.063	0.069	0.065	**0.060**	-0.107	-0.099	-0.096	**-0.094**	-0.095
TxSON	0.85	0.85	0.84	0.84	**0.85**	**0.033**	0.034	0.036	0.038	0.033	**-0.056**	-0.060	-0.063	-0.057	-0.059
USCRN	**0.74**	0.73	0.70	0.71	0.73	0.049	0.049	0.051	0.051	**0.049**	-0.057	-0.053	-0.053	**-0.050**	-0.053
iRON	0.44	**0.48**	0.40	0.38	0.48	0.051	0.050	0.052	0.052	**0.050**	-0.114	-0.110	-0.113	-0.109	**-0.107**
Median	**0.67**	0.67	0.64	0.65	0.67	**0.058**	0.059	0.063	0.063	0.059	-0.067	-0.061	-0.062	**-0.056**	-0.061
Optimal/All	3/23	7/23	1/23	0/23	**12/23**	**10/23**	2/23	0/23	2/23	9/23	3/23	1/23	1/23	**11/23**	7/23

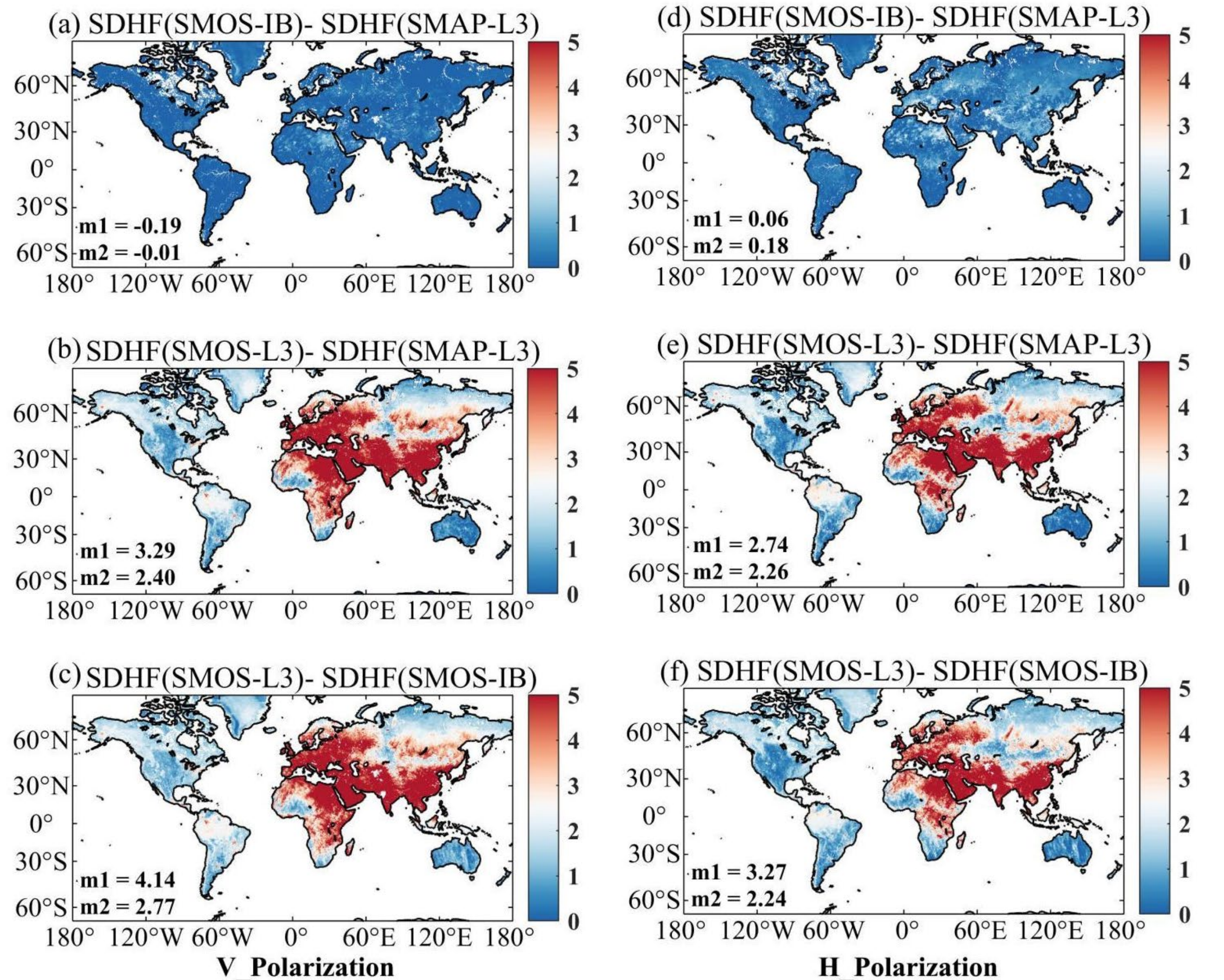

Figure S1 Maps of the standard deviation of the high-frequency variations (SDHF) difference of the TB time series for each of the three TB products in V-polarization (a) - (c) and H-polarization (d) - (f). The TB SDHF were computed after removing the seasonal trend that was estimated with a 30-days moving window average filter. m1 and m2 denote the spatial mean and median SDHF difference value, respectively.

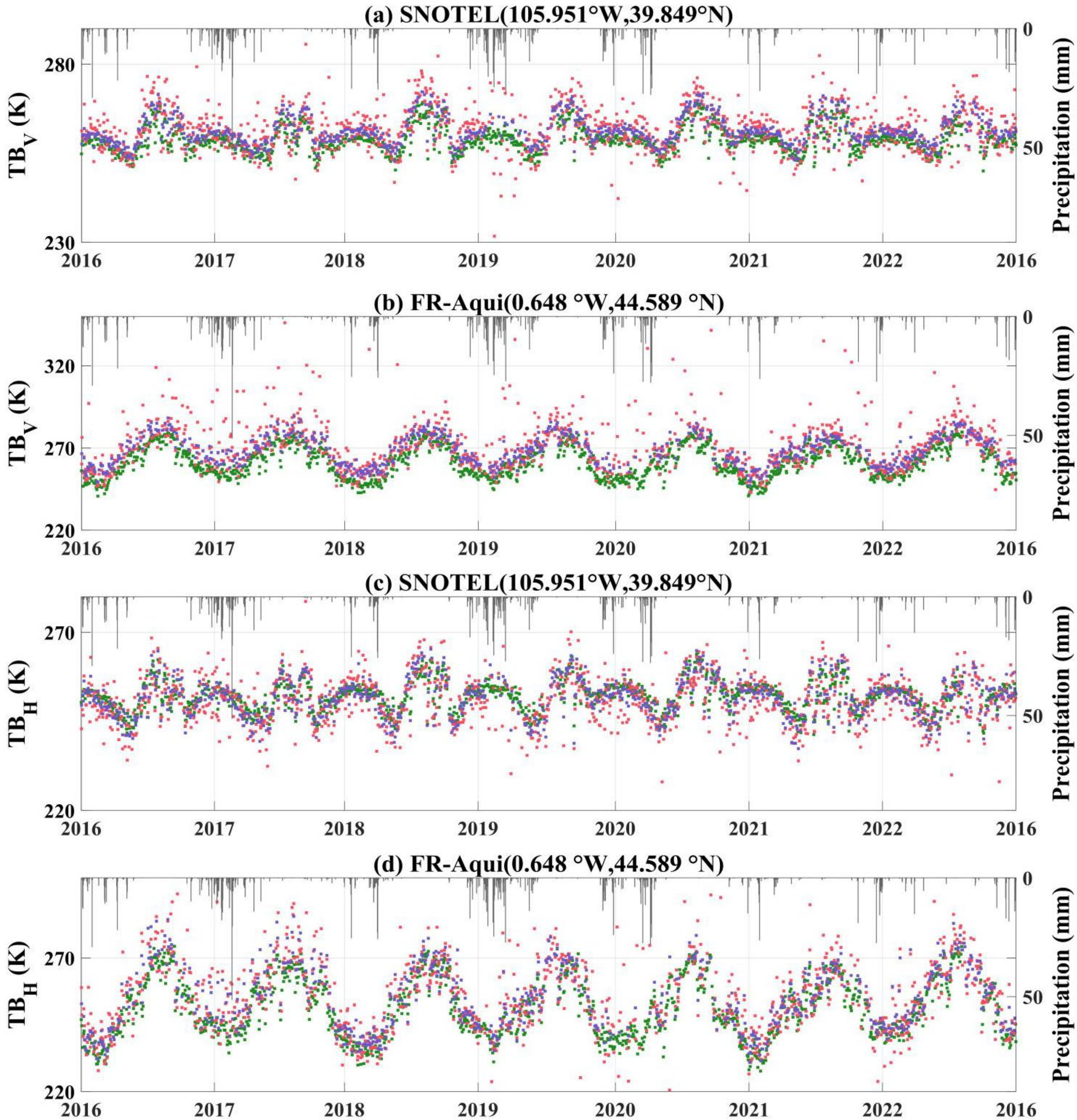

Figure S2 Time series of the three TB products and *in-situ* measurements between 2016 and 2022 at two sites from (a) SCAN and (b) FR-Aqui network, respectively. Each plot also contains daily precipitation shown in the axis on the right side (grey bar).

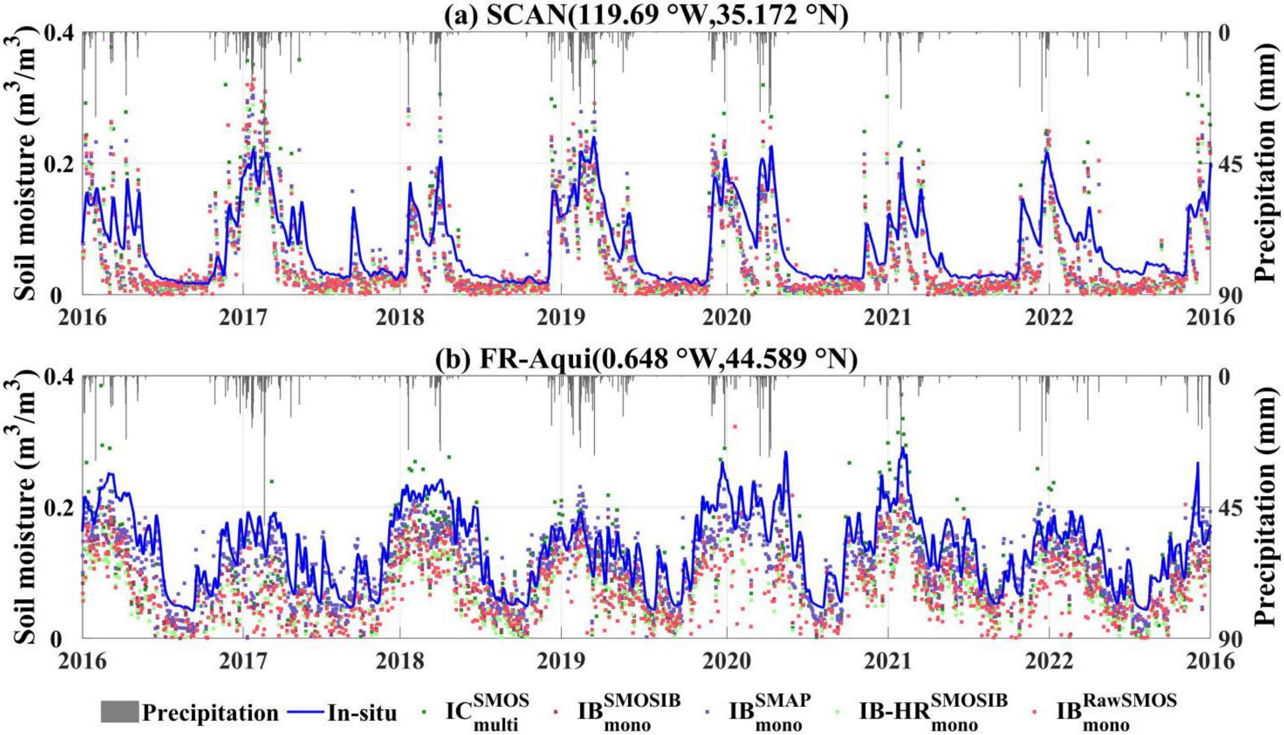

Figure S3 Time series of the five SM products and *in-situ* measurements between 2016 and 2022 at two sites from (a) SCAN and (b) FR-Aqui network, respectively. Each plot also contains daily precipitation shown in the axis on the right side (grey bar). Note that a 7-day moving window filter was applied to the i*n-situ* observations to distinguish them from the satellite-based SM.

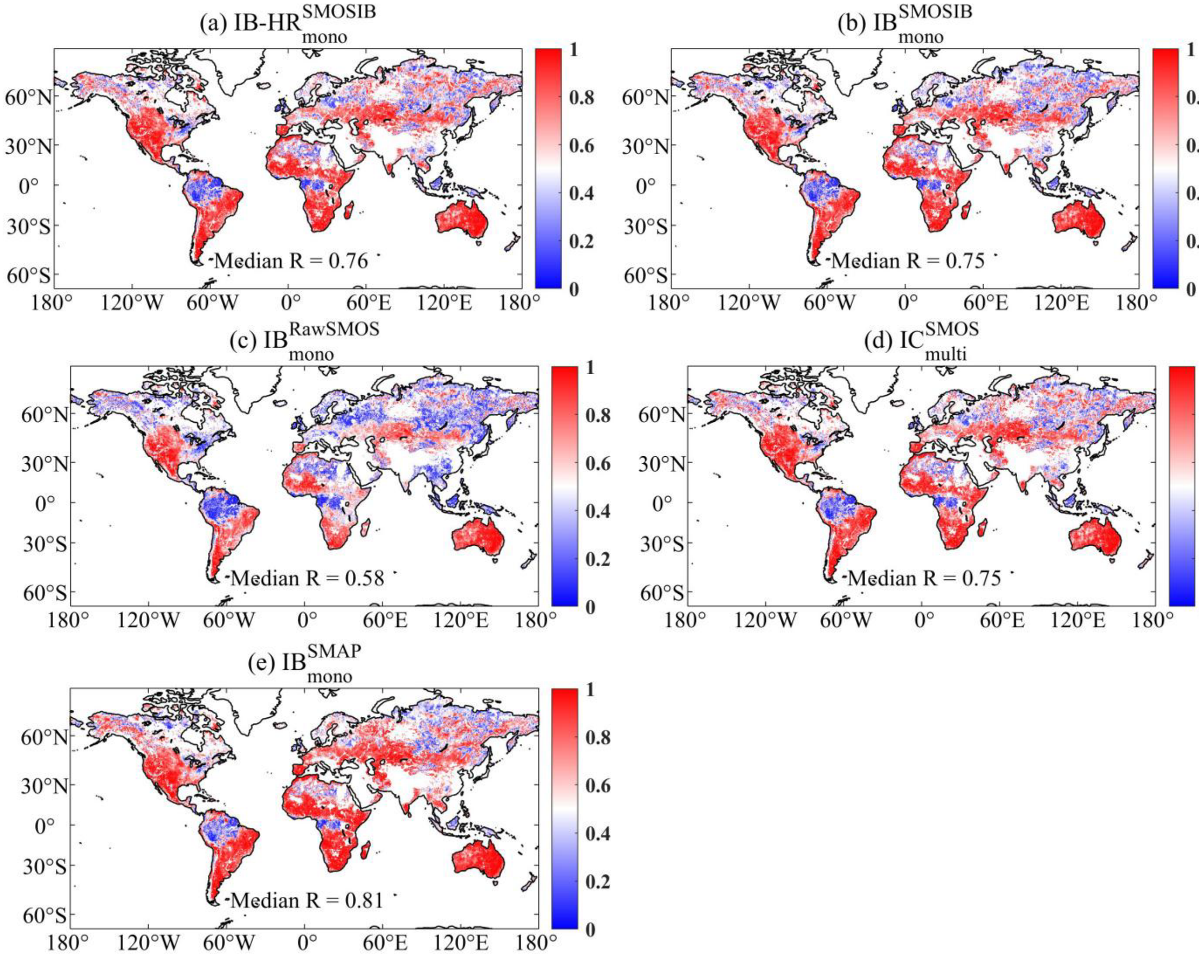

Figure S4 The spatial distribution of the TCA-based R calculated by soil moisture anomaly estimates for (a) $IB\_HR_{mono}^{SMOSIB}$, (b) IB_{mono}^{SMOSIB}, (c) $IB_{mono}^{RawSMOS}$, (d) IC_{multi}^{SMOS} and (e) IB_{mono}^{SMAP}.

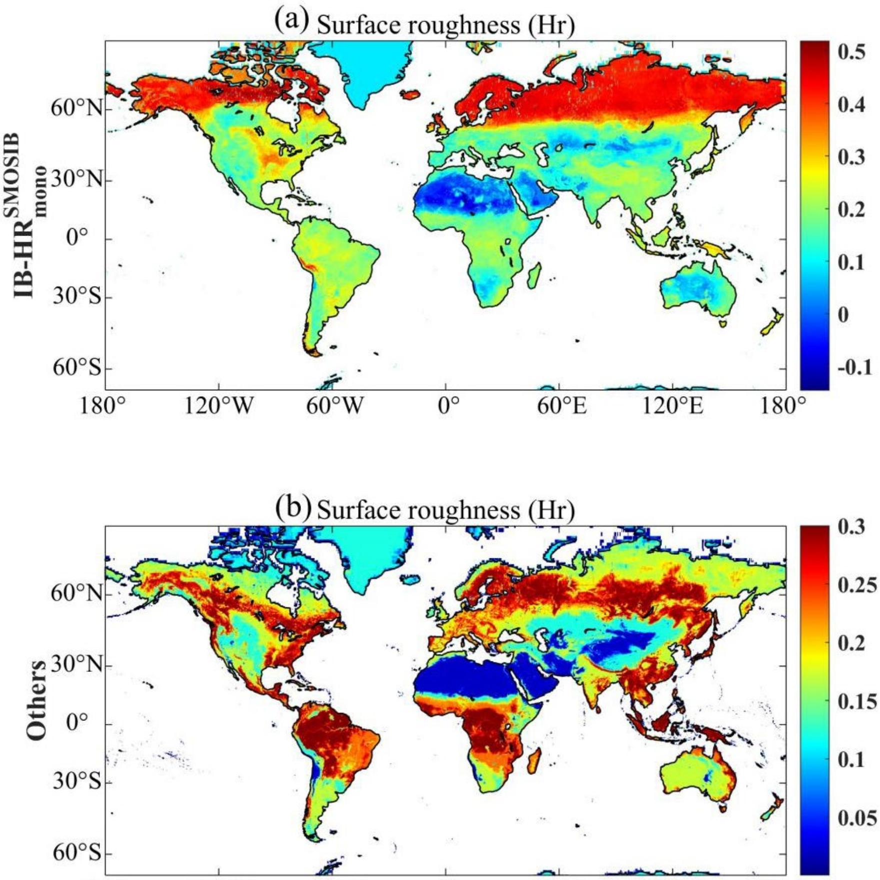

Figure S5 The spatial distribution of input Hr values for (a) $IB\_HR_{mono}^{SMOSIB}$ and (b) other products (*e.g.,* IB_{mono}^{SMOSIB}, $IB_{mono}^{RawSMOS}$, IC_{multi}^{SMOS} and IB_{mono}^{SMAP}).

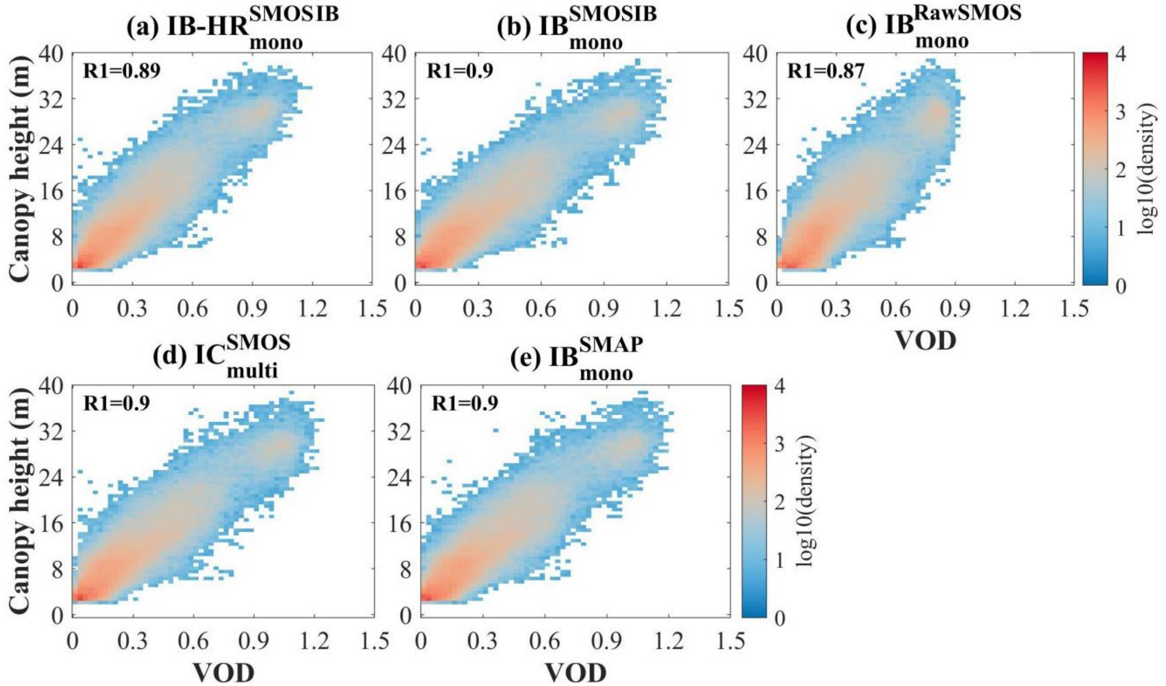

Figure S6 Global density plots of VOD vs. canopy height (a-e) for five products: (a)$IB\_HR^{SMOSIB}_{mono}$, (b) IB^{SMOSIB}_{mono}, (c) $IB^{RawSMOS}_{mono}$, (d) IC^{SMOS}_{multi} and (e) IB^{SMAP}_{mono}. *R1* denotes the correlation coefficient computed spatially between VOD and corresponding proxies.

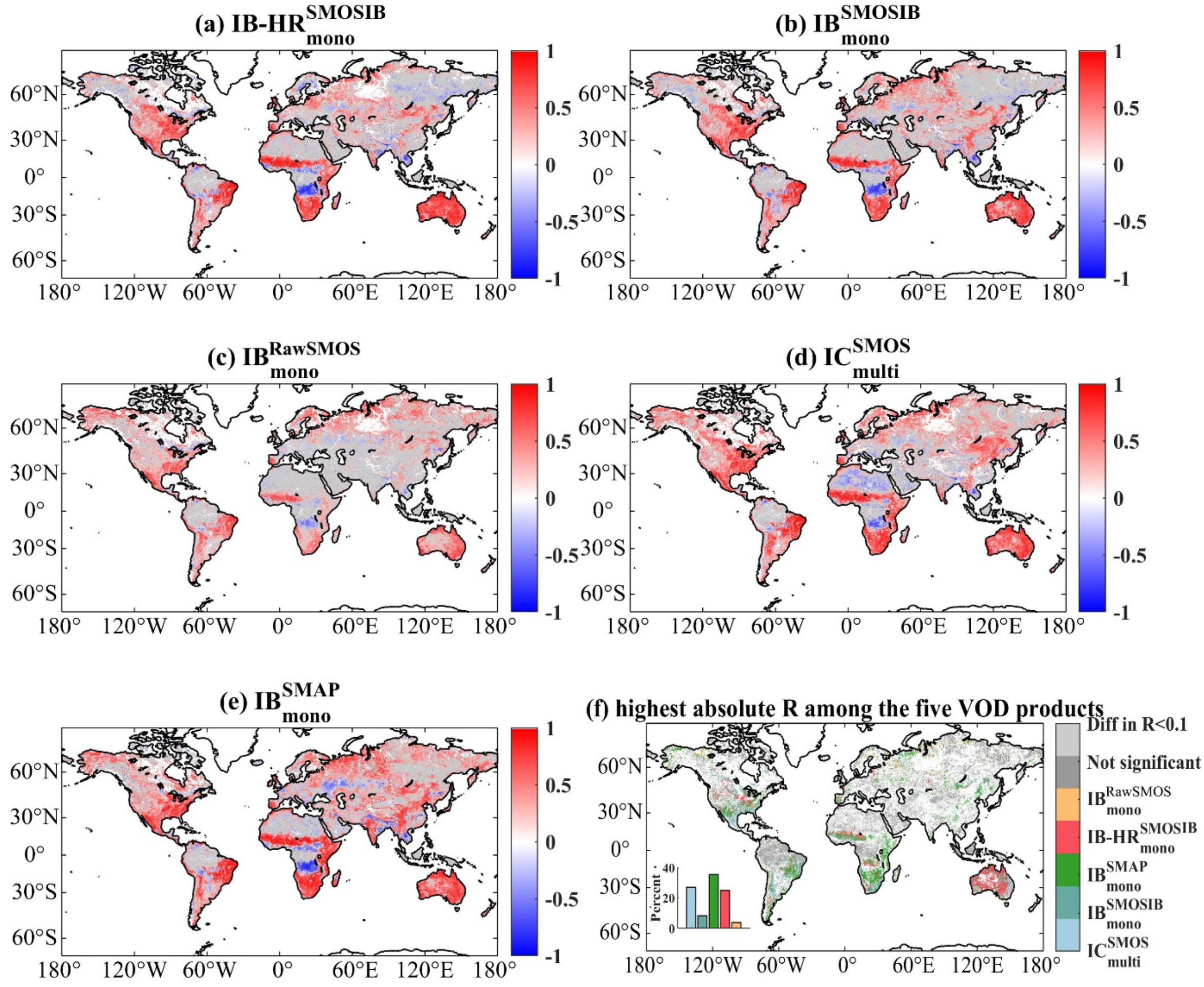

Figure S7 Correlation coefficient (R) of the temporal relationship between 16-day composite of VOD and NDVI (2016 – 2022) for (a) $IB\_HR^{SMOSIB}_{mono}$, (b) IB^{SMOSIB}_{mono}, (c) $IB^{RawSMOS}_{mono}$, (d) IC^{SMOS}_{multi} and (e) IB^{SMAP}_{mono}. (f) maps of the above five VOD datasets with the highest absolute R values with NDVI. The dark grey color indicates pixels with non-significant ($p > 0.05$) R values, and the light grey color indicates pixels with R difference for each paired VOD product < 0.1. White areas mean "no valid data".

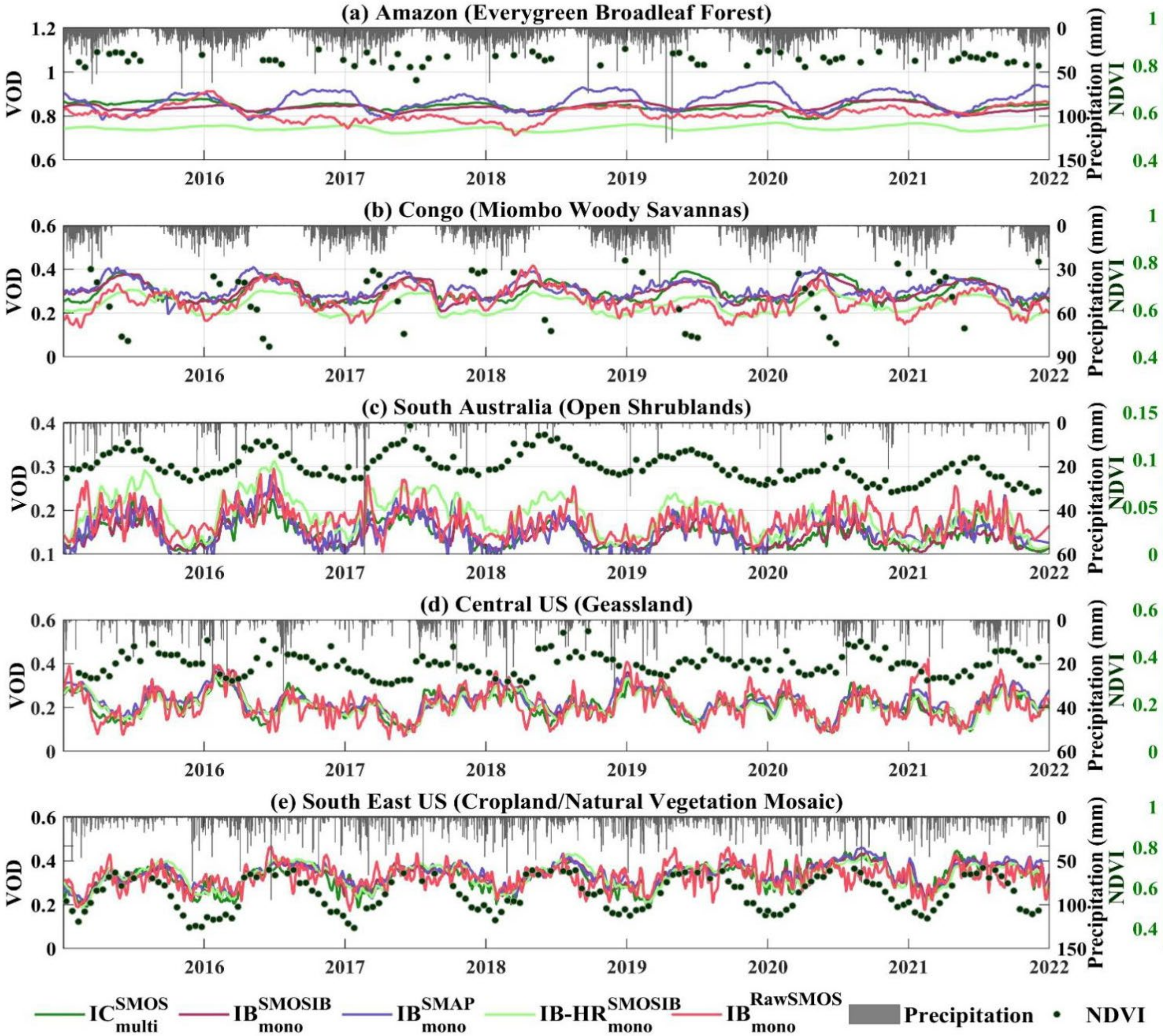

Figure S8 Time series of the five VOD products over five pixels corresponding to (a) Everygreen broadleaf forest (64.79 °W, 6.65 °S), (b) Miombo woody savannas (23.71 °E, 8.85 °S), (c) Open shrublands (124.54 °E, 30.31 °S), (d) Grasslands (110.39 °W, 34.31 °N) and (e) Cropland/Natural vegetation mosaic (86.83 °W, 35.34 °N) between Jan 2016 and Dec 2022. Each plot also contains daily precipitation and NDVI information. Note that a 7-day moving window filter was applied to the VOD values of the five products to distinguish them from the NDVI values.